北京大学学报(自然科学版), 第 50 卷, 第 4 期, 2014 年 7 月
Acta Scientiarum Naturalium Universitatis Pekinensis, Vol. 50, No. 4 (July 2014)
doi: 10.13209/j.0479-8023.2014.115

Improved Structure of Time-Divided Closed-Loop Accelerometer by Alternating the Voltage Biasing

HUANG Jingqing, ZHAO Meng, ZHANG Tingting, CHEN Zhongjian, WU Feng,
HONG Lichen, LIU Dahe, ZHANG Yacong†, LU Wengao, GAO Chengchen, HAO Yilong

National Key Laboratory of Science and Technology on Micro/Nano Fabrication, Institute of Microelectronics,
Peking University, Beijing 100871; † Corresponding author, E-mail: zhangyc@pku.edu.cn

Abstract A new structure of time-divided closed-loop accelerometer is proposed. It requires only one operational amplifier as a negative-coefficient PID is just sufficient. This structure not only reduces the area consumption of the whole chip of the readout circuit, but also lowers the equivalent input noise acceleration as one operational amplifier and two large resistors are reduced. The readout circuit is fabricated using 0.35 μm HV CMOS process, with self-test function included. Test results show that the linearity of 99.72% is achieved under self-test mode. The root-mean-square output noise voltage is around 140 μV from DC to 200 Hz.

Key words proportional integral derivative controller; closed-loop; accelerometer; self-test function; microelectromechanical systems

偏置电压交变的时分反馈闭环加速度计

黄靖清 赵猛 张婷婷 陈中建 伍峰 洪理琛 刘大河 张雅聪†
鲁文高 高成臣 郝一龙

北京大学微纳电子学系微纳米/纳米加工技术国家级重点实验室, 北京 100871; † 通信作者, E-mail: zhangyc@pku.edu.cn

摘要 提出一种改进结构的时分反馈闭环加速度计, 该结构使用负系数的 PID 控制器, 只需要一个运算放大器。改进后的结构减小了读出电路的芯片面积, 同时省去一个运算放大器和两个大电阻, 因此能降低系统噪声。读出电路采用 0.35 μm 高压 CMOS 工艺, 并包含自检测功能。测试结果显示, 在自检测模式下, 闭环加速度计的线性度为 99.72%。在 DC 到 200 Hz 内, 输出噪声电压均方根值约为 140 μV。

关键词 比例积分微分控制器; 闭环; 加速度计; 自检测; 微机电系统

中图分类号 TN432

An accelerometer mainly consists of a microelectromechanical systems (MEMS) sensor and a CMOS readout integrated circuit (ROIC). When better linearity, resolution and higher signal band are required, closed-loop accelerometer are chosen over open-loop ones. This electromechanical hybrid system forms a closed-loop by exploiting electrostatic force[1–2], which is also applied for self-test function[3–4].

To achieve the stability of the closed-loop system, a proportional integral derivative (PID) controller is usually essential. The PID is generally composed of multiple operational amplifiers, resistors and capacitors[5]. The most intuitive positive-coefficient PID needs as much as five amplifiers[6].

Various methods have been reported to implement closed-loop accelerometers[7–9]. Time-divided method has been chosen as it gives much freedom to control the voltage biasing of the MEMS sensor. This

---

863 计划(2008AA042201)资助
收稿日期: 2013–04–06; 修回日期: 2014–02–17; 网络出版日期: 2014–07–13

advantage is essential for the improved time-divided closed-loop accelerometer, which is adapted from a conventional one. By carefully redesigning the biasing of the MEMS sensor, the improved structure eliminates the need of analog inverter which is part of positive-coefficient PID. Therefore, area consumption of the ROIC chip is reduced and noise performance is also enhanced.

1 Closed-Loop Accelerometer of Conventional Time-Divided Structure

1.1 Overall structure of the conventional closed-loop accelerometer

The conventional structure of time-divided closed-loop accelerometer is shown in Fig. 1. This accelerometer consists of a MEMS sandwich capacitive sensor and a CMOS ROIC. Particularly the ROIC is composed of charge sensitive amplifier (CSA), sample and hold circuit (S&H), low pass filter (LPF), PID and a voltage buffer (BUF).

The feedback switch shown in Fig. 1 divides each period of the accelerometer into two different phases, the detecting phase and the feedback phase. The ROIC detects the acceleration signal from the sensor during the detecting phase, and applies electrostatic force on the sensor during the feedback phase.

As the accelerometer responds to acceleration signals from DC to several hundred Hertz, the low frequency noise performance is crucial. Therefore, CSA which directly faces MEMS sensor is of much importance when noise is taken into consideration. Correlated double sampling (CDS) is exploited in CSA. According to the block diagram shown in Fig. 1, a more detailed schematic based on operational amplifiers is illustrated in Fig. 2.

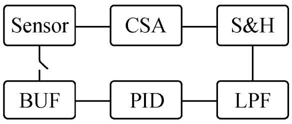

Fig. 1 Overall structure of conventional time-divided closed-loop accelerometer

1.2 Necessity of a positive-coefficient PID

MEMS sandwich capacitive symmetrical sensor shown in Fig. 1 is modeled as a pair of differential capacitors as shown in Fig. 2. A more detailed model is shown in Fig. 3.

Capacitances of top and bottom capacitors are

$$C_1 = \frac{\varepsilon_0 A}{d_0 - x}, \tag{1}$$

$$C_2 = \frac{\varepsilon_0 A}{d_0 + x}, \tag{2}$$

where ε_0 is vacuum permittivity, A is the capacitance overlapping area, d_0 is the distance between the proof mass and the top or bottom plate, x is the displacement of the proof mass. Therefore, the differential capacitance is

$$\Delta C = C_1 - C_2 = \frac{2\varepsilon_0 A}{d_0^2 - x^2} \cdot x\,. \tag{3}$$

The pulses that are fed into the top and bottom electrodes of the MEMS sensor are periodical. Their

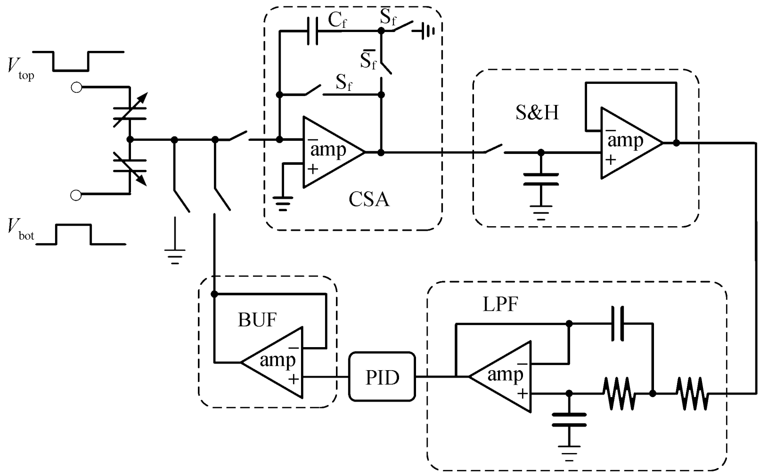

Fig. 2 Operational amplifier based schematic of conventional time-divided closed-loop accelerometer

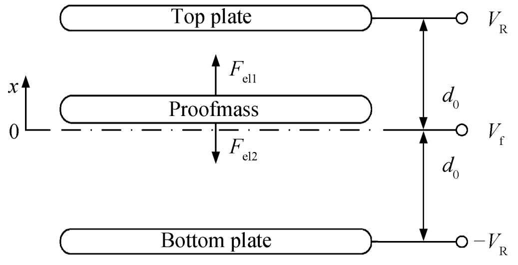

Fig. 3　Model MEMS sandwich capacitive sensor

waves are illustrated in Fig. 4.

In the detecting phase, when x is small compared with d_0, the output of CSA is

$$V_{CSA} = \frac{\Delta C \cdot V_R}{C_f} = \frac{2\varepsilon_0 A V_R}{C_f \cdot d_0^2} \cdot x. \tag{4}$$

In the feedback phase, the top electrode of the sensor is biasing at a positive voltage V_R, while the bottom electrode is $-V_R$. Therefore, the electrostatic forces of F_{el1} and F_{el2} as illustrated in Fig. 3 are

$$F_{el1} = \frac{\varepsilon_0 A}{2} \frac{(V_R - V_f)^2}{(d_0 - x)^2}, \tag{5}$$

$$F_{el2} = \frac{\varepsilon_0 A}{2} \frac{(-V_R - V_f)^2}{(d_0 + x)^2}, \tag{6}$$

where V_f is output voltage of BUF. When x is small compared with d_0, resultant force of F_{el1} and F_{el2} is

$$F_{el} = F_{el2} - F_{el1} = \frac{2\varepsilon_0 A V_R}{d_0^2} \cdot V_f. \tag{7}$$

F_{el} is meant to balance the inertial force F_i. Therefore F_{el} must be positive when x is positive and negative when x is negative. Eq. (7) clearly shows that the sign of F_{el} is the same of the sign of V_f.

As can be easily seen from schematic shown in Fig. 2, the sign of V_f is determined by PID, whose transfer function is

$$H(s)_{PID} = P + \frac{I}{s} + D \cdot s. \tag{8}$$

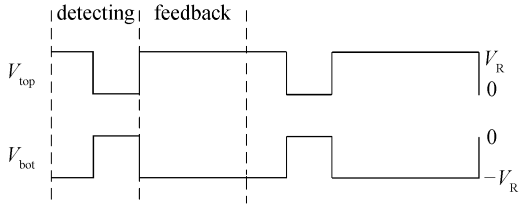

Fig. 4　Waves fed into the top and bottom electrodes of sensor

Therefore, P, I and D should all be positive. Fig. 5 shows the conventional way to realize a positive-coefficient PI, whose parameter D is zero.

This positive-coefficient PI actually consists of a negative-coefficient PI and an analog inverter. The analog inverter adds a phase shift of 180°, which is required for the stability of the closed-loop system.

2　Closed-Loop Accelerometer of Improved Time-Divided Structure

2.1　Overall structure of the improved closed-loop accelerometer

The analog inverter is composed of an operational amplifier and two large resistors and consumes a considerably large area. However, its main function is adding a phase shift of 180°. If this function can be realized by some other way, the analog inverter can be omitted.

After carefully examining Eq. (7), it is found that the direction of the electrostatic force can be easily turned opposite by simply substituting $-V_R$ for V_R. If so, the waves shown in Fig. 4 should be modified to those shown in Fig. 6.

Therefore, analog inverter is no longer needed in closed-loop and overall structure of improved time-divided accelerometer is attained as shown in Fig. 7.

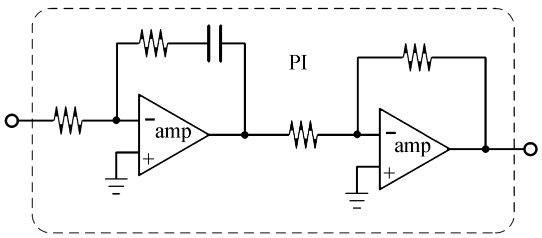

Fig. 5　Conventional positive-coefficient PI

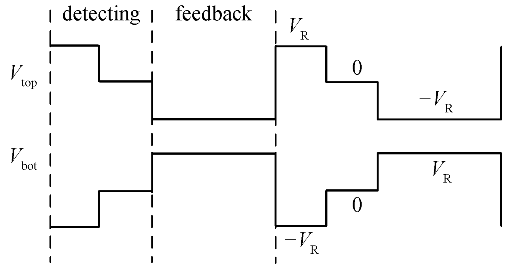

Fig. 6　Waves fed into the top and bottom electrodes of sensor under the improved time-divided structure

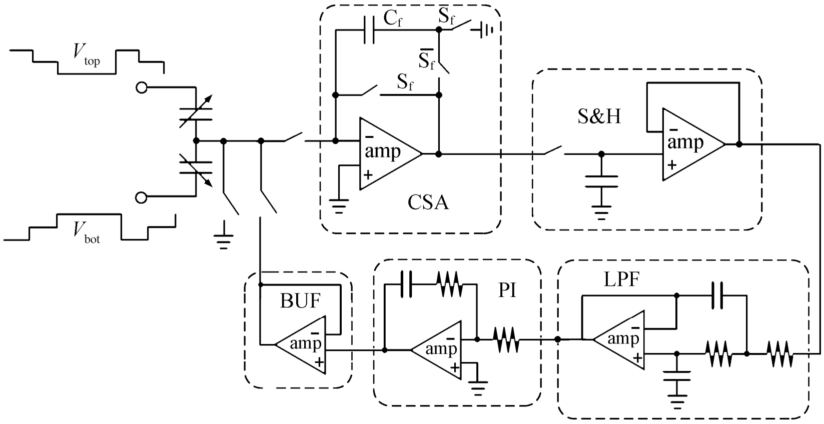

Fig. 7 Operational amplifier based schematic of improved time-divided closed-loop accelerometer

Compared with the conventional structure, the improved structure saves the area of an operational amplifier and two large resistors with minor modification of the digital logic. Moreover, noises of these three components are all eliminated.

2.2 Self-test mode

For testability and easy-to-test design, a self-test mode is added to the accelerometer. Under this mode, each period of the working frequency is divided into three phases. A self-test phase is inserted between detecting phase and feedback phase as shown in Fig. 8.

In the self-test phase, an external voltage is connected to the ROIC through pad. This would apply electrostatic force on the proof mass of the MEMS sensor so as to simulate the inertial force caused by an acceleration signal.

3 Test Results

The closed-loop of the accelerometer is designed according to Fig. 7 with minor modification by adding self-test mode. The whole ROIC is designed and fabricated using 0.35 μm HV CMOS process, and consumes an area of around 4.3 mm by 2.3 mm. The photograph of ROIC is shown in Fig. 9.

Time-divided closed-loop accelerometer is formed by integrating MEMS sensor and ROIC together on a PCB as shown in Fig. 10. Exploiting this accelerometer, self-test function is tested. As depicted in Fig. 11, test results show that linearity of 99.72% is achieved under self-test mode. Noise level of the output of ROIC is measured under normal air pressure as shown in Fig. 12. The root-mean-square output noise voltage is around 140 μV from DC to 200 Hz.

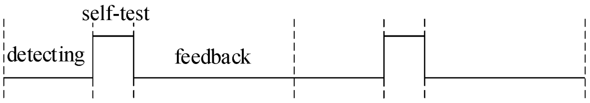

Fig. 8 Three phases under self-test mode

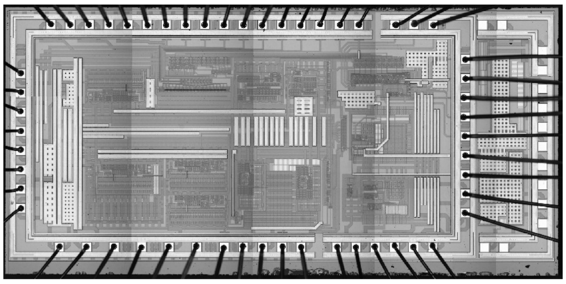

Fig. 9 Photograph of the ROIC

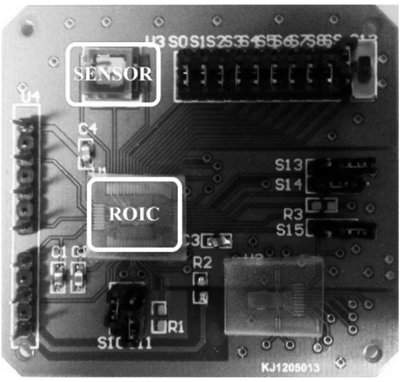

Fig. 10 Photograph of PCB as closed-loop accelerometer

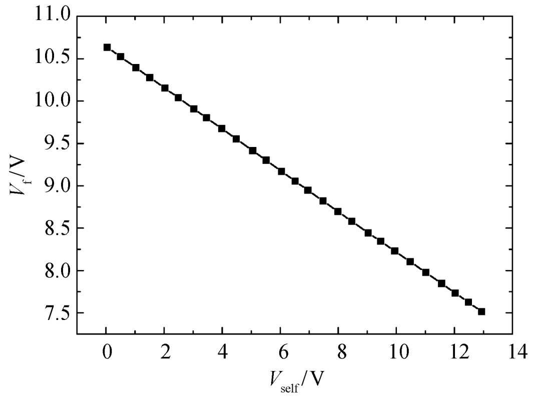

Fig. 11　Test results of self-test function

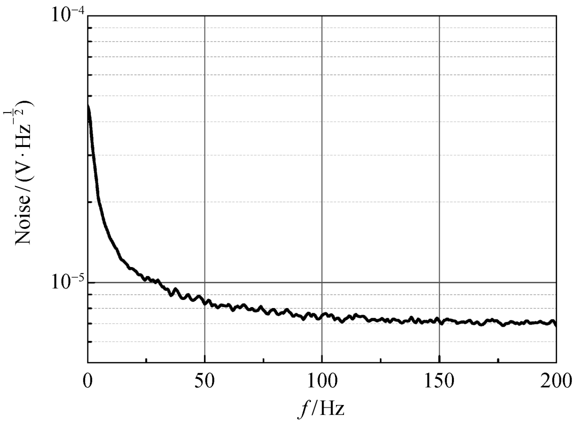

Fig. 12　Noise level of improved time-divided closed-loop accelerometer

4　Conclusion

An improved structure of time-divided closed-loop accelerometer is presented. The improved structure, by alternating the voltage biasing of top and bottom electrodes of MEMS sensor, maintains a stable closed-loop system. Therefore, area consumption of the analog inverter is saved and the noises of this block are eliminated at the meantime. For testability and easy-to-test design, self-test mode is added. ROIC of this improved structure is fabricated using 0.35 μm HV CMOS process. Test results of self-test function and noise performance are given.

References

[1] Yücetas M, Pulkkinen M, Kalanti A, et al. A high-resolution accelerometer with electrostatic damping and improved supply sensitivity. IEEE Journal of Solid-State Circuits, 2012, 47(7): 1721–1730

[2] Külah H, Chae J, Yazdi N, et al. Noise analysis and characterization of a Sigma-Delta capacitive micro-accelerometer. IEEE Journal of Solid-State Circuits, 2006, 41(2): 352–361

[3] Wei C Z, Zhou W, Wang Q, et al. Monolithic pressure+acceleration sensor with self-test function for reliable & low-cost tire-pressure-monitoring-system (TPMS) applications // 16th International Solid-State Sensors, Actuators and Microsystems Conference (TRANSDUCERS). Beijing, 2011: 1006–1009

[4] Deb N, Blanton R D. Built-in self-test of MEMS accelerometers. IEEE Journal of Microelectrome-Chanical Systems, 2006, 15(1): 52–68

[5] Aaltonen L, Rahikkala P, Saukoski M, et al. High-resolution continuous-time interface micromachined capacitive accelerometer. International Journal of Circuit Theory and Applications, 2009, 37: 333–349

[6] Grigorie T L. The Matlab/Simulink modeling and numerical simulation of an analogue capacitive micro-accelerometer. Part 2: closed loop // International Conference on Perspective Technologies and Methods in MEMS Design. Polyana, 2008: 115–121

[7] Paavola M, Kämäräinen M, Laulainen E, et al. A micropower ΣΔ-based interface ASIC for a capacitive 3-axis micro-accelerometer. IEEE Journal of Solid-State Circuits, 2009, 44(11): 3193–3210

[8] He Lin, Xu Yongping, Palaniapan M. A CMOS readout circuit for SOI resonant accelerometer with 4-μg bias stability and 20-μg per rtHz resolution. IEEE Journal of Solid-State Circuits, 2008, 43(6): 1480–1490

[9] Liu Yuntao, Liu Xiaowei, Yin Liang, et al. CMOS interface circuitry for a closed-loop capacitive MEMS accelerometer // Proceedings of 4th IEEE International Conference on Nano/Micro Engineered and Molecular Systems. Shenzhen, 2009: 510–513